AIAA JOURNAL
Vol. 44, No. 1, January 2006

Active Control of Separation from the Flap of a Supercritical Airfoil

LaTunia Pack Melton* and Chung-Sheng Yao†
NASA Langley Research Center, Hampton, Virginia 23681
and
Avi Seifert‡
Tel-Aviv University, 69978 Ramat-Aviv, Israel

Zero-net-mass-flux periodic excitation was applied at several regions on a simplified high-lift system to delay the occurrence of flow separation. The NASA Energy Efficient Transport supercritical airfoil was equipped with a 15% chord simply hinged leading-edge flap and a 25% chord simply hinged trailing-edge flap. Detailed flow features were measured in an attempt to identify optimal actuator placement. The current paper describes the application of active separation control at several locations on the deflected trailing-edge flap. High- and low-frequency amplitude modulation of the high-frequency excitation were used for control. It was noted that the same performance gains were obtained with amplitude modulation and required only 30% of the momentum input required by pure sine excitation. Extreme sensitivity was found to the excitation location where the flap is highly curved. This sensitivity was reduced when using low-frequency amplitude modulation due to the long wavelengths generated by the excitation. It was found that for large flap deflections the majority of the lift increasing alteration of the surface pressures results from an upstream effect. Preliminary results of combining the excitations from leading- and trailing-edge devices are also presented.

Nomenclature

C_D = total drag
C_{dp} = pressure drag coefficient
C_L = lift coefficient
$C_{L,\max}$ = maximum lift coefficient
C_p = pressure coefficient, $(P - P_s)/q$
$C_{p,\min}$ = minimum pressure coefficient
C_μ = oscillatory excitation momentum coefficient, $\equiv J'/cq$
c = model chord
F^+ = reduced frequency, $\equiv (f x_{\mathrm{sp}})/U_\infty$
f = oscillation frequency, Hz
h = slot height or width
J' = oscillatory momentum at slot exit, $\rho h u_j^2$
M = Mach number
P = pressure
P_s = static pressure
q = freestream dynamic pressure, $1/2\rho U_\infty^2$
Re_c = chord Reynolds number, $U_\infty c/\nu$
T = temperature
U = averaged streamwise velocity
u = standard deviation of fluctuating streamwise velocity
x/c = normalized streamwise location
x_{sp} = distance from actuator to trailing edge (TE)
z = spanwise location
α = angle of attack
δ_f = TE flap deflection angle
δ_s = leading-edge flap deflection angle
δ^* = boundary-layer displacement thickness, $\int_0^\infty \left(1 - \frac{\rho U}{\rho_e U_e}\right) \mathrm{d}y$
ν = kinematic viscosity
ρ = density

Subscripts

e = boundary-layer edge
j = conditions at excitation slot
S = separation
∞ = freestream conditions

Presented as Paper 2003-4005 at the AIAA 33rd Fluid Dynamics Conference, Orlando, FL, 23–26 June 2003; received 15 July 2004; revision received 4 May 2005; accepted for publication 11 May 2005.

*Research Engineer, MS 170, Flow Physics and Control Branch; l.p.melton@larc.nasa.gov. Member AIAA.
†Research Scientist, MS 170, Flow Physics and Control Branch; c.s.yao@larc.nasa.gov.
‡Senior Lecturer, Department of Fluid Mechanics and Heat Transfer, School of Mechanical Engineering, Faculty of Engineering; also Visiting Scientist, National Institute of Aerospace, 100 Exploration Way, Hampton, VA 23666; seifert@eng.tau.ac.il. Associate Fellow AIAA.

Introduction

ACTIVE flow control using periodic excitation has been investigated by numerous researchers in the past decade.[1–6] The interest in periodic excitation is due to technological advances that reduce the complexity of integrating it on a flight vehicle combined with experimental results that show the ability of periodic excitation to effectively control flow separation.[3–5] One of the primary advantages of periodic excitation for separation control is that the technique is momentum efficient when compared to steady momentum transfer methods. The efficiency of periodic excitation is due in part to exciting the flow at frequencies that correspond to natural instabilities of the separating shear layer. Another advantage of periodic excitation is that zero-net-mass-flux excitation can be used, thereby eliminating the need to connect the actuation system to an auxiliary compressor or a vacuum system. Effective and efficient flow separation control can be achieved using zero-net-mass-flux devices that require only electrical inputs. A comprehensive review of the history of flow separation control by periodic excitation can be found in Ref. 1, whereas a more recent review can be found in Ref. 7.

This paper focuses on the use of periodic excitation via zero-net-mass-flux excitation for controlling separation on a simplified high-lift system. The goal of the experiment is to determine whether a supercritical airfoil with simply hinged leading-edge (LE) and trailing-edge (TE) flaps, equipped with periodic excitation for flow

separation control, can match the performance of a conventional multi-element high-lift system. The efficiency of the latter stems from passive slots and the Fowler effect used for generating the high lift. A system study performed by McClean et al.[8] indicated that, by simplifying a conventional high-lift system, manufacturing cost could be reduced by 0.66%, weight reduced by 2.8%, and drag reduced by 3.1%. One percent of the drag reduction was due to the possible elimination of large, drag-producing external flap hinges and positioning actuators. These numbers are based on having hinged LE and TE flaps and accounting for the flow control system. The current model design that uses only simply hinged LE and TE flaps enables the complete elimination of hinges and positioning actuators that are external to the airfoil contour, at the cost of losing the passive slots between airfoil elements for energizing the boundary layers. This should be compensated for by active boundary-layer (BL) control.

The current paper deals with TE flap separation control; the results obtained when applying excitation at the LE flap shoulder of this airfoil were documented in a previous publication.[6] High-frequency excitation, typical of the piezoelectric actuators currently used, applied at the LE flap shoulder, delayed stall and increased $C_{L,\max}$ by 10–15% at low TE flap deflections. It was shown that low-frequency amplitude modulation (AM) could be used to achieve similar benefits in aerodynamic performance and allow a reduction of the oscillatory momentum input by 50–70%. Once the danger of encountering laminar LE stall was eliminated, we focused our attention on controlling TE flap separation.

Because of the large TE flap deflections that might be required to match the performance of the multi-element version of this airfoil, several actuation locations on the TE flap were independently investigated. The paper focuses on the sensitivity of the control process to actuation location, Reynolds number, and excitation frequency. Finally, the combination of LE and TE flow control is examined with the aim of evaluating the capability of active separation control to replace passive boundary-layer energization by slots.

Experiment

Wind Tunnel

The test was conducted in the Basic Aerodynamic Research Tunnel (BART) at NASA Langley Research Center. The BART facility is a low-speed open-circuit wind tunnel, with a 0.71-m-high × 1.02-m-wide × 3.05-m-long test section. The maximum speed of the tunnel is 60 m/s ($Re/m = 0.345 \times 10^6$). The wind tunnel is well instrumented and allows optical access for the performance of particle image velocimetry (PIV).

Simplified High-Lift Model

The simplified high-lift version of the NASA Energy Efficient Transport (EET) airfoil[6,9] was designed in a modular manner so that zero-net-mass-flux actuators could replace solid regions in the model near the LE and TE flap shoulders (Fig. 1a). The 406.4-mm-chord model has a 15% chord LE flap that can be deflected from 0 to −30 deg and a 25% chord TE flap that can be deflected from 0 to 60 deg. Angle-of-attack settings for the airfoil and the two flaps were automated and closed-loop computer controlled. The model has 78 streamwise static pressure taps located at midspan and two rows of 18 spanwise static pressure taps spaced 50.8 mm apart located at $x/c = 0.35$ and $x/c = 0.94$ on the upper surface. In addition to the static pressure taps, there are nine unsteady pressure transducers on the model surface and at least one unsteady pressure transducer embedded in each actuator cavity. The unsteady pressure transducer is used to monitor the pressure fluctuations produced by the actuator and to correlate the wind-tunnel experiments with the bench-top actuator calibration tests.

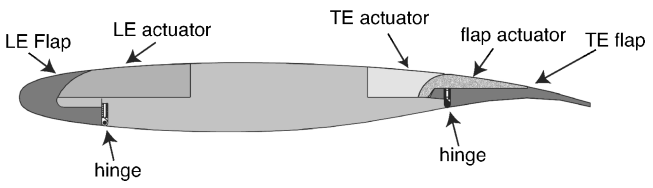

a) Actuator regions of EET model

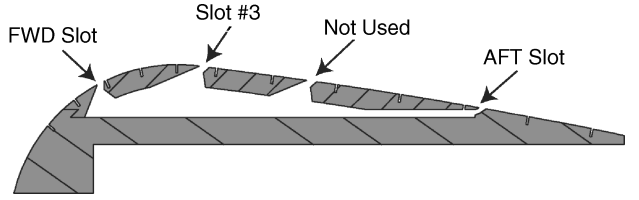

b) Internal piezoelectric flap actuator cross section

Fig. 1 Modified EET model.

Table 1 Flap actuator slot locations

Slot	x/c location at $\delta_f = 0$ deg
FWD	0.725
3	0.757
Not used	0.790
Aft	0.845

Flap Actuator

An internal piezoelectric actuator was used on the TE flap (Fig. 1). The flap actuator, with its four alternative excitation slots, all inclined at about 30 deg to the surface and directed downstream, is shown in Fig. 1b. The three upstream slots are 0.635 mm wide, and the aft slot is 0.51 mm wide. The x/c locations for the flap actuator slots ($\delta_f = 0$ deg) are given in Table 1.

The three forward slots are segmented (19 segments, 0.051 m in length) and the aft slot is continuous. A comprehensive bench-top calibration, using a single hot wire that was traversed at 0.127-m intervals along the span of each slot with all other slots sealed, was performed. The standard deviations across the entire span of the velocity rms values near resonance at the maximum actuator input voltage, 40 V_{rms}, were 19, 21, and 28%, respectively, for the FWD (Fig. 1b), slot 3, and aft slots. Unsteady pressures were measured in the actuator's cavity to monitor its operation during the calibration and while in the tunnel. The oscillatory momentum coefficient for the pure sine wave and AM cases was then based on the velocity rms (u) computed using the correlation between cavity pressure and velocity defined using the bench-top calibration data. The flap actuator was operated at its resonant frequency (1 kHz ± 0.3 kHz, depending on the slot used) using a pure sine wave and using AM via a sine wave at frequencies lower than the actuator's resonant frequency by an order of magnitude. Only one slot was active during each experiment. The three forward slots were sealed using a water-soluble filler to minimize surface discontinuities, and kapton tape, 0.051 mm thick and 12.7 mm wide, was used to seal the aft slot.

Particle Image Velocimetry Setup

Two-dimensional digital PIV was used to measure the instantaneous flowfields, phase-synchronized with the flap actuator cycle (when active). The PIV system includes two 1024 × 1024 pixel cameras installed side by side with a 105-mm macro lens. The fields of view from the two cameras were overlapped to capture the entire TE flap region. The width of the measurement plane was about 120 mm. A non rectangular grid was used with a minimum resolution of 24 × 24 pixels. The maximum overlap between adjacent interrogation regions was 50%. Smoke, introduced upstream of the open-loop wind-tunnel contraction, was used for seeding. Dual Nd-Yag lasers were used to illuminate a light sheet, placed about 50 mm to the left side of the model centerline (facing upstream).

Experimental Uncertainty

The airfoil incidence angles, α, are accurate to within ±0.03 deg. The LE and TE flap deflection angles are accurate to within ±0.25 deg, C_μ is accurate to within 20% (partly due to slot width uncertainty of ±0.08 mm and partly due to calibration uncertainties such as sensor location and ±2% uncertainty in hot-wire velocity

Table 2 Uncertainty of airfoil integral parameters

Parameter	Fully attached	Stalled	Controlled
C_L	0.01	0.04	0.02
C_{dp}	0.002	0.004	0.003
C_D	0.002	0.008	0.006

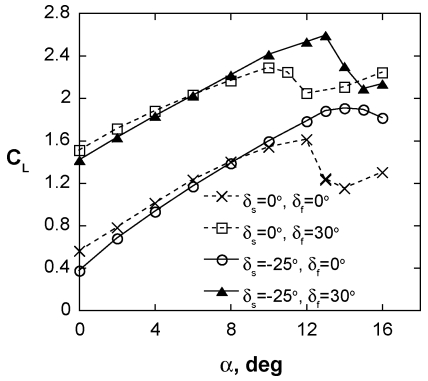

Fig. 2 Lift coefficients of the EET airfoil at different high-lift configurations as tested in BART at $Re_c = 0.75 \times 10^6$.

measurements), and Re_c is accurate to within 3%. The uncertainties of the airfoil integral parameters are listed in Table 2 (in absolute values and related to flow conditions).

The large uncertainty in the total drag C_D is due to the extrapolation of the wake data for some of the high-lift configurations of the airfoil, to wind-tunnel interference, and to uncertainty about wind-tunnel static pressure at the wake rake location. It should be noted that the integral parameters in this paper were not corrected for the significant tunnel wall interference effects present in the BART facility for the model size used; however, the relative improvement in performance is believed to be conservative.

Test Conditions (Flow and Geometry)

The majority of the experiments using the TE flap were conducted at incompressible Mach numbers and values of Re_c ranging from 0.24×10^6 to 0.75×10^6. The flap deflections were varied from $\delta_f = 0$ to 60 deg for the TE and $\delta_s = 0$ to -30 deg for the LE flaps, respectively.

Results

The baseline (no-control) performance of the airfoil is discussed in Ref. 6. Some of the relevant baseline data are repeated and discussed here for completeness. The purpose of deflecting the LE flap was to eliminate the possibility of LE separation due to the low radius of curvature of the LE.[10] In application, it will be required to consider both large and small LE and TE flap deflections for typical landing and takeoff conditions, respectively.

Lift data for a candidate landing configuration ($\delta_f = 30$ deg and $\delta_s = -25$ deg) are shown in Fig. 2. The following data are also included in this figure: data for the cruise configuration ($\delta_f = \delta_s = 0$ deg), data for $\delta_f = 0$ deg at $\delta_s = -25$ deg (showing delayed and milder stall), and data for $\delta_f = 30$ deg at $\delta_s = 0$ deg (showing increased lift and earlier stall). The lift data for the $\delta_f = 30$ deg, $\delta_s = -25$ deg configuration indicate that the LE flap effect is almost added to the TE flap effect and that the stall "milding" capability of the LE flap is maintained even at $\delta_f = 30$ deg. The challenge is now to apply periodic excitation on both LE and TE flap shoulders to delay BL separation at both actuator locations allowing larger LE and TE flap deflections and thereby enhanced lift.

Effects of the Active TE Flap Excitation Slot Location

A summary of the major findings with regard to the optimal location for the introduction of periodic excitation, keeping in mind that the aim is to increase the effectiveness of the TE flap, is given in Fig. 3 for $\alpha = 0$ deg. In all cases considered, the separating BL was turbulent. The aft slot, located at $x/c = 0.845$ (when $\delta_f = 0$ deg), becomes effective for $\delta_f > 5$ deg, reaches optimal performance at $\delta_f = 12$ deg, and loses its effectiveness at $\delta_f > 20$ deg, where the separation point moves upstream of the aft slot. Slot 3, situated roughly $9\%c$ upstream of the aft slot, starts being effective at $\delta_f \approx 10$ deg, reaches its peak performance at $\delta_f \approx 20$ deg, and stops being effective at $\delta_f > 30$ deg, for the same reason as the aft slot. The FWD slot is exposed to the external flow only for $\delta_f > 22$ deg (Fig. 1a) and becomes effective only for $\delta_f > 30$ deg, peaks at $\delta_f \approx 50$ deg, and losses effectiveness at $\delta_f \approx 60$ deg. The effective range of each slot vs δ_f is not significantly sensitive to C_μ or to F^+ (using $F^+ > 4$) or to Re_c, as shown by the data (Fig. 3). A small adverse effect at the edges of the effective range of each slot is also shown in Fig. 3. Such effects were not seen when using low F^+ excitation or LE excitation, and the source of this effect is unknown. Note that the small difference in slot locations ($\Delta x/c \approx 3.2\%$; see Fig. 1b and Table 1) between the FWD slot and slot 3, results in a 30-deg change in δ_f for max effectiveness of the two slots. For comparison the difference between the aft slot and slot 3 ($\Delta x/c \approx 9\%$) results in only an 8-deg difference in δ_f for maximum effectiveness. A possible explanation for this significant finding is that the FWD slot region has surface curvature, whereas the upper TE flap surface, downstream of slot 3, is almost flat.

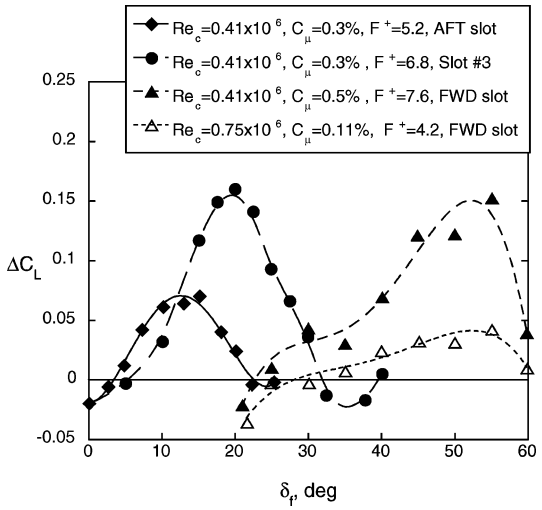

Fig. 3 Lift increment vs TE flap deflection angle for different slot locations (shown in Fig. 1b; $\alpha = 0$ deg, $\delta_s = 0$ deg).

TE Flap Forward Slot Excitation

Figure 4a shows the lift increment and form drag alteration due to high F^+, pure sine excitation, and AM of the $F^+ = 13$ excitation at $F^+_{AM} = 0.32$ (note curve-fitted data). The choice of this F^+_{AM} will be explained later. The data of Fig. 4a clearly show that larger lift increments are generated between $\delta_f = 30$ and 50 deg when using $F^+_{AM} = 0.32$ rather than using $F^+ = 13$, reducing the effective δ_f range of the TE flap FWD slot by about 10 deg, with respect to the pure sine, high-frequency excitation. However, the high F^+ excitation without AM reduces the form drag more effectively throughout the δ_f range. This finding indicates that it should be possible, by changing only the excitation frequency, to alter the lift-to-drag ratio while maintaining lift and to obtain similar effects as would be obtained by altering the excitation slot location. These effects are hypothesized to be related to the ratio between the convective low F^+_{AM}, long-wavelength excitation and the radius of curvature of the surface at the excitation slot and the flow separation region. The data indicate that the longer-wavelength vortical structures generated by the $F^+_{AM} = 0.32$ excitation are less sensitive to the curvature of the TE flap surface.

The increase in form drag when using the F^+_{AM} excitation may be due to exciting the flow near the natural vortex shedding frequency (VSF). Naim et al.[11] and Naim[12] have shown that excitation

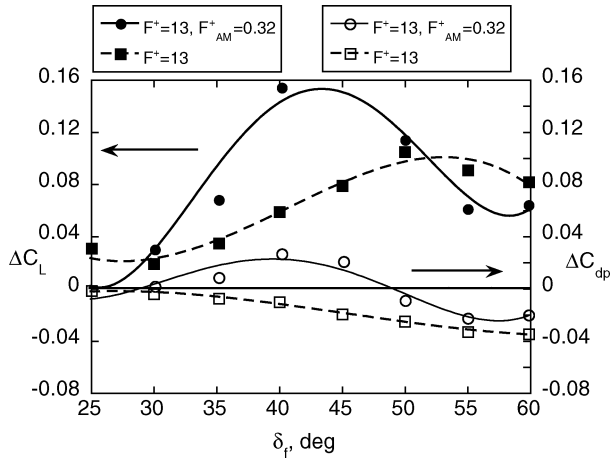

a) ΔC_L and ΔC_{dp} as a function δ_f

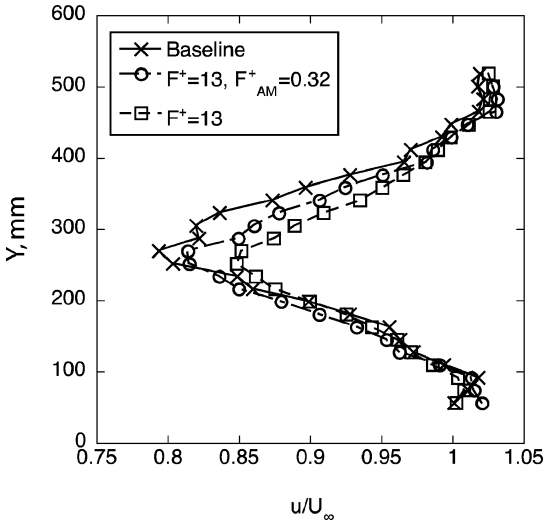

c) Wake distribution ($\delta_f = 45$ deg)

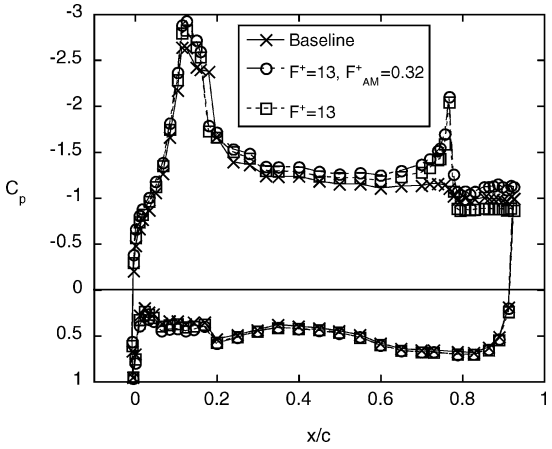

b) Pressure distribution ($\delta_f = 45$ deg)

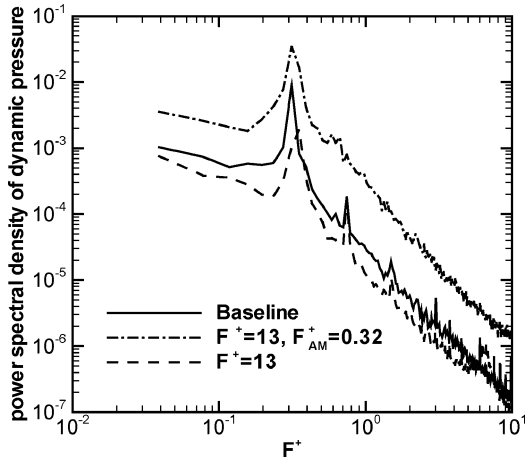

d) Flap TE pressure spectra ($\delta_f = 45$ deg).

Fig. 4 TE flap FWD slot control ($Re_c = 0.24 \times 10^6$, $\alpha = 0$ deg, $\delta_s = -25$ deg, $C_\mu = 0.38\%$).

at frequencies close to the natural VSF increases the drag of bluff-bodies. This occurs due to closer forming and more energetic von Kármán vortices in the wake of the separated bluffbody. The aforementioned effect induces a stronger upstream directed flow (in a frame of reference advected with the body) and hence larger drag. It remains to be seen if a similar mechanism is active in separated flow over conventional airfoils as well. The natural VSF of the baseline flow data, described in Figs. 4b and 4c, can be deduced from the pressure spectra measured at the TE, shown in Fig. 4d. The baseline data show a distinct natural peak at $F^+ \approx 0.3$.

The C_p distributions and wake velocity profiles at $\delta_f = 45$ deg are presented in Figs. 4b and 4e and provide further insight into the effects of the excitation on C_L and C_{dp}. The data of Fig. 4b indicate that the low-F^+_{AM} and the high-F^+ excitations have the opposite effect on the upper-surface TE flap pressures. The average $C_p(x/c = 0.79$ to the TE) on the TE flap of the baseline flow is -0.984. Low-F^+_{AM} excitation reduces the average C_p on the TE flap to -1.097 and high-F^+ excitation increases the average C_p to -0.876. The low-F^+ AM excitation mostly generates an upstream effect that is responsible for the lift increment at high δ_f, where complete TE flap flow reattachment is impossible with the available C_μ. The larger C_p on the TE flap generated by the high-F^+ pure sine wave excitation is beneficial for drag reduction (Fig. 4c). This is attributed to the larger pressure on the negatively sloped TE flap upper surface, indicated by the narrower wake and the slightly higher VSF (Fig. 4d, $F^+ = 13$). From the available data it seems that the high-F^+ excitation delays separation, narrows the wake, increases the VSF, and reduces the form drag (Figs. 4b–4d). The AM excitation increases

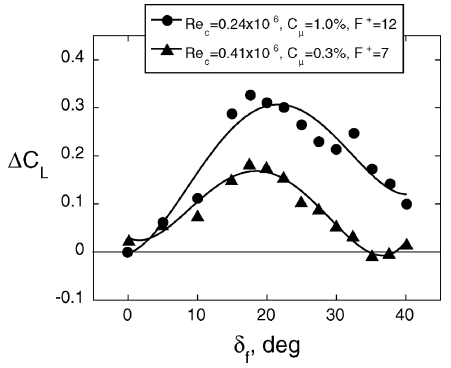

Fig. 5 Reynolds number effect on lift increment vs TE flap deflection angle ($\alpha =$ deg, $\delta_s = -25$ deg, flap slot 3).

the magnitude of the VSF (Fig. 4d; closer and stronger vortices as indicated by a stronger spectral peak). The VSF "locks" to the AM F^+ and increases the form drag for $\delta_f \leq 50$ deg (Fig. 4a). Note that the total drag, predicted from the wake momentum deficit for the AM data, is less reliable due to the low-frequency oscillation of the wake flow, as indicated by the TE pressure spectra (Fig. 4d).

TE Flap Slot 3 AFC Results

The lift increment vs TE flap deflection angle for excitation emanating from slot 3 at $Re_c = 0.24 \times 10^6$ and 0.41×10^6 is presented in Fig. 5. The data shown in Fig. 5 indicate that the Re_c and F^+,

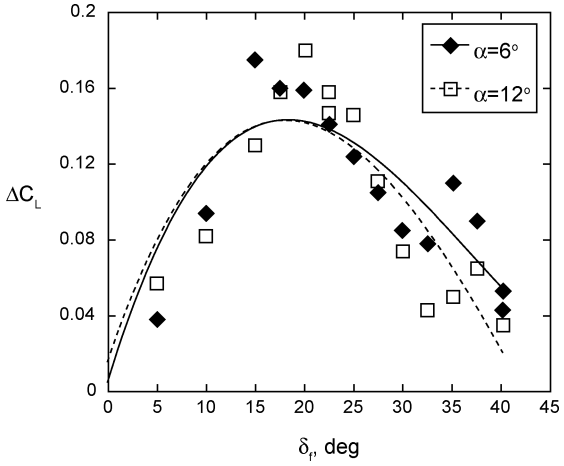

Fig. 6 Angle-of-attack effect on lift increment vs TE flap deflection angle ($Re_c = 0.24 \times 10^6$, $\delta_s = -25$ deg, $C_\mu = 1.0\%$, $F^+ = 12$, flap slot 3).

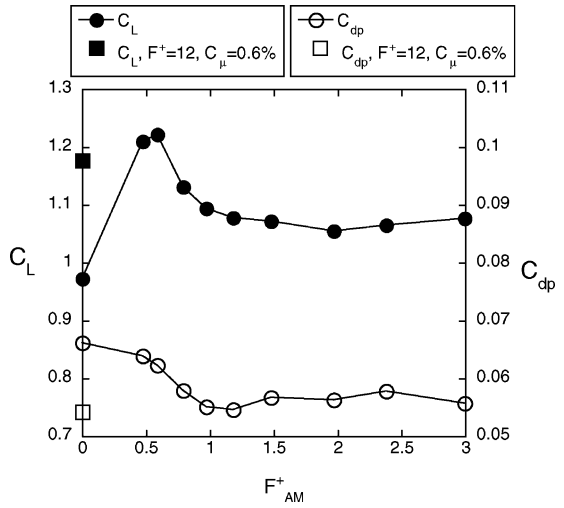

Fig. 7 Effect of F^+_{AM} on C_L and C_{dp} ($\alpha = 0$ deg, $\delta_s = -25$ deg, $\delta_f = 20$ deg, flap slot 3, see Fig. 1b; $Re_c = 0.24 \times 10^6$, $C_{\mu,\mathrm{AM}} = 0.2\%$).

in the range presented, have a weak effect on the optimal δ_f of slot 3 excitation. Also, for approximately triple the value of C_μ, only twice the lift increment is obtainable at the lower Re_c. In Fig. 6, the effect of airfoil angle of attack on optimal δ_f for slot 3 is examined at $Re_c = 0.24 \times 10^6$. The data indicate that the airfoil incidence angle has no effect on the optimal TE flap deflection or on the attainable lift increment when using slot 3 with $\delta_s = -25$ deg. This finding is encouraging when attempting to increase $C_{L,\max}$ of a high-lift airoil.

As already mentioned in the context of Fig. 4, low-frequency modulation of the high-F^+ excitation increases the lift-generating capability of the TE flap flow forcing mechanism while generally increasing rather than decreasing the form drag. Detailed AM frequency scans are presented and discussed in this section.

Figure 7 shows the effect of variations in F^+_{AM} on the lift and form drag, with excitation introduced from slot 3, using $C_{\mu,\mathrm{AM}} = 0.2\%$. The geometry and Reynolds number were $\alpha = 0$ deg, $\delta_s = -25$ deg, $\delta_f = 20$ deg, and $Re_c = 0.24 \times 10^6$, respectively. The AM data are compared to pure sine, high-F^+, high-C_μ (0.6%) data (plotted as square symbols at $F^+_{\mathrm{AM}} = 0$). Note that triple the C_μ using pure sine excitation generates approximately the same variation in lift and form drag as the optimal low F^+_{AM}. Also, the optimal values of F^+_{AM} are different for the lift increment (without form drag reduction) and form drag reduction (at half the lift increment). The optimal reduced AM frequencies are $F^+_{\mathrm{AM}} \approx 0.5$ for lift increment and $F^+_{\mathrm{AM}} \approx 1$ for form drag reduction. The F^+ sensitivity data are consistent with the pure harmonic, low-frequency scan performed by Seifert et al.[3] for lift increment purposes. The form drag reduction found at twice the optimal ΔC_L frequency was also observed by Naim et al.[11,12]

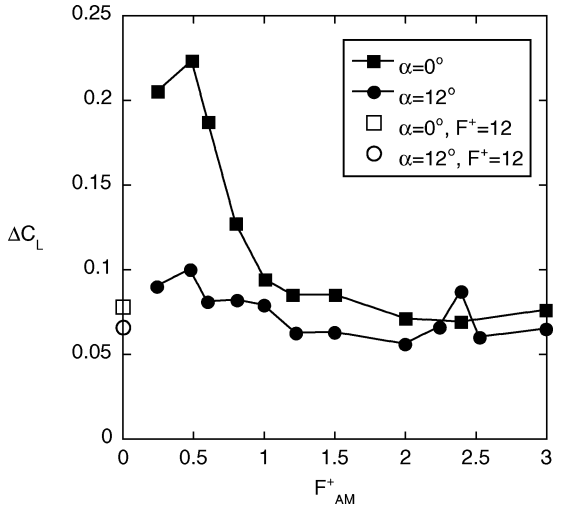

Fig. 8 F^+_{AM} effect ($Re_c = 0.24 \times 10^6$, $\delta_f = 20$ deg, $\delta_s = -25$ deg, flap slot 3, $C_\mu = 0.2\%$).

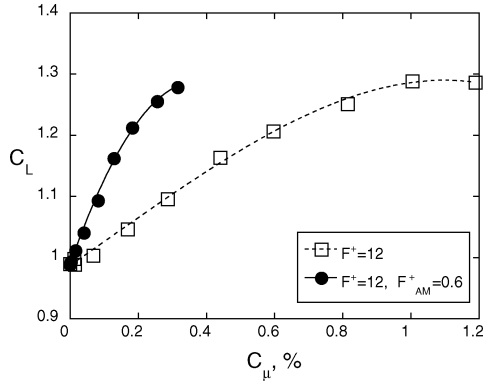

a) C_μ effect on C_L

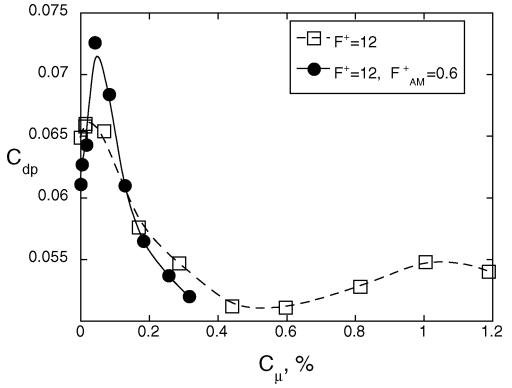

b) C_μ effect on C_{dp}

Fig. 9 Amplitude scan (flap slot 3, $Re_c = 0.24 \times 10^6$, $\delta_s = -25$ deg, $\delta_f = 20$ deg, $\alpha = 0$ deg).

Figure 8 presents the lift increment vs F^+_{AM} at $\alpha = 0$ deg and $\alpha = 12$ deg ($C_{L,\max}$ of the baseline) with excitation introduced from slot 3. The data indicate, in agreement with Seifert and Pack,[4] that the lift increment is approximately halved (using the same C_μ) when approaching $C_{L,\max}$, but the effective F^+_{AM} remains unchanged though less distinct. The reduction in the effectiveness of the excitation for lift increment is attributed to an increase in the BL thickness, larger adverse pressure gradient on the TE flap, and the intermittently separated flow at the slot location.

Figure 9a shows the lift and Fig. 9b shows the form drag, comparing the effects of the magnitude of the pure sine, high-frequency

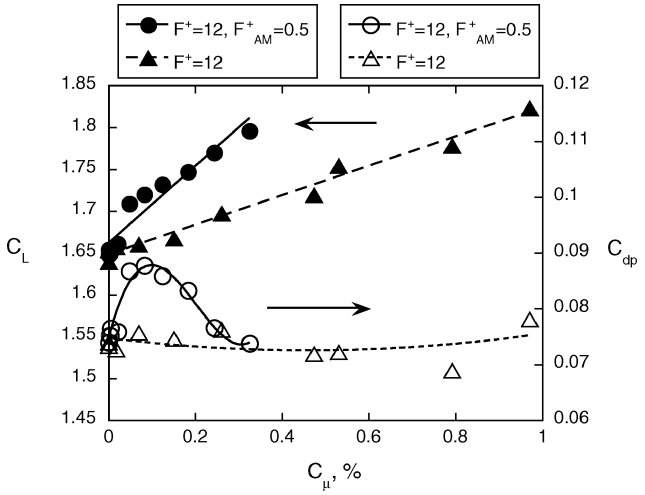

a) Amplitude scan

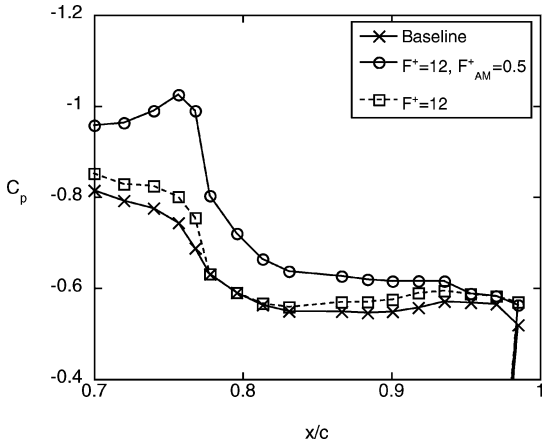

b) C_p plot at $C_\mu \approx 0.08\%$

Fig. 10 Effect of pure sine control and AM control on C_L and C_{dp} (flap slot 3, $Re_c = 0.24 \times 10^6$, $\alpha = 6$ deg, $\delta_s = -25$ deg, $\delta_f = 20$ deg).

excitation to those due to $F^+_{AM} = 0.6$ excitation. The data shown in Fig. 9 indicate that only a third of the C_μ is required to generate the same increment in lift when using $F^+_{AM} = 0.6$. The form drag (Fig. 9b) initially increases for low levels of C_μ (more significantly for $F^+_{AM} = 0.6$); however, for $C_\mu > 0.15\%$ the trend of the drag data is similar, regardless of the excitation signal frequency content.

Figure 10a shows data similar to those of Fig. 9a, but at a larger incidence angle of $\alpha = 6$ deg. The low F^+_{AM} is still more energy efficient, but the form drag is not increased by using high-frequency excitation. It requires, again, roughly only a third of the C_μ to generate the same ΔC_L. Drag is not reduced by the available range of C_μ, which is incapable of even partially reattaching the flow to the TE flap at this α and δ_f. The $F^+ = 12$ excitation and the $F^+_{AM} = 0.5$ excitation have a similar effect (though weaker for $F^+ = 12$) on the C_p distribution upstream of $x/c = 0.70$; therefore, the data are omitted from Fig. 10b. When observing the C_p variations due to AFC on the TE flap upper surface, the F^+_{AM} excitation decreases the pressure on the TE flap more than the $F^+ = 12$ excitation, increasing both C_L and C_{dp}. The TE flap upper-surface average C_p values from $x/c = 0.8$ to the TE are -0.56 for the baseline, -0.62 for the $F^+ = 12$, $F^+_{AM} = 0.5$ excitation and -0.58 for the $F^+ = 12$ excitation.

Flow Details

To better explore flow modifications due to the excitation and correlate these to variations in the BL separation location and eventually to alterations of the aerodynamic performance of the wing in the high-lift configuration, flow physics details need to be studied and understood. For this purpose, C_p data are correlated with flowfield data acquired by PIV and will be discussed in this section.

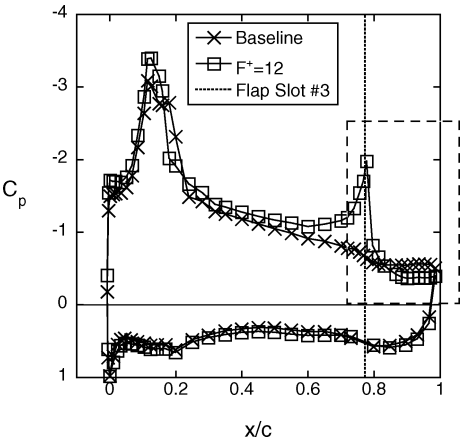

a) C_p distribution

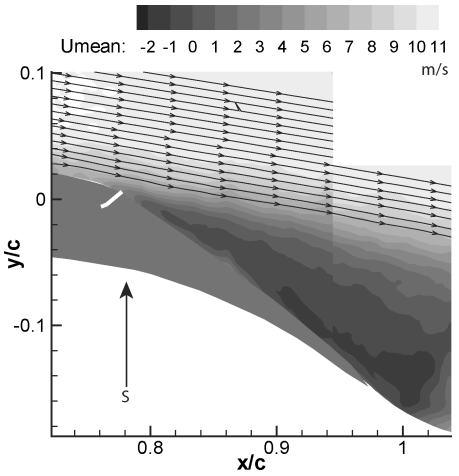

b) PIV baseline

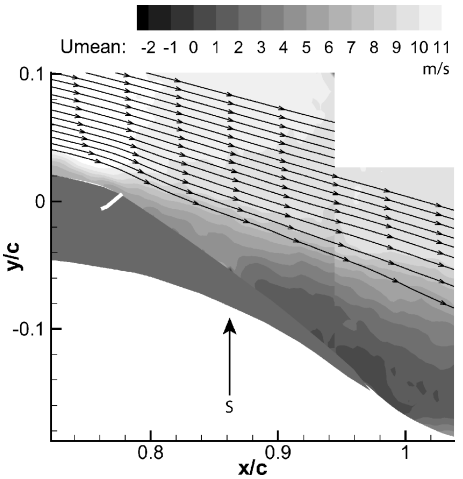

c) PIV controlled ($F^+ = 12$, $C_\mu = 1.0\%$)

Fig. 11 Baseline and controlled flowfield ($Re_c = 0.24 \times 10^6$, $\alpha = 6$ deg, $\delta_s = -25$ deg, $\delta_f = 20$ deg, $F^+ = 12$, $C_\mu = 1.0\%$); arrows shown in PIV images indicate x/c location of separation on upper surface of model.

Figure 11a shows the C_p distributions of the baseline and $F^+ = 12$ controlled flowfields at $\alpha = 6$ deg. The excitation is introduced from slot 3, indicated by the vertical, dotted line superimposed on the C_p plot at $x/c = 0.78$. A strong suction peak was established at the slot and upstream acceleration was induced due to the excitation. The flow on the TE flap is partially reattached resulting in $\Delta C_L = 0.17$ and $\Delta C_{dp} = 0.004.0$ (The excitation increases both C_L and C_{dp} at this condition.) The excitation on the TE flap also promotes laminar–turbulent transition on the LE flap. This presumably happens due to

the increased circulation over the entire airfoil, which generates a more severe adverse pressure gradient or by acoustic radiation from the TE flap excitation to the LE separation bubble. The length of the separation bubble seen at $x/c = 0.20$ in the baseline C_p distribution is reduced (Fig. 11a). The dashed box in Fig. 11a represents the region where the PIV data were acquired (refer only to the x/c bounds) and these data are presented in Figs. 11b and 11c. The PIV data, acquired using two partially overlapping cameras, show that the baseline flow separates from the TE flap at $x/c \approx 0.8$ (Figs. 11b and 11c) and the separated streamline flows at an angle of about -10 deg with respect to the freestream direction. When excitation from slot 3 is introduced, separation is delayed to $x/c \approx 0.9$ and the separating streamline angle is about -23 deg. Note that the inclination of the upper surface of the TE flap is about -36 deg. The induced upstream acceleration is demonstrated by the reduction in the BL displacement thickness, δ^*/c, at $x/c = 0.74$ from 0.015 in the baseline to 0.008 in the controlled flow.

Combination of LE and TE Control

To effectively use the potential of the simplified high-lift system, separation should be controlled on both the LE and TE flap shoulders. The role of the LE actuator would be mostly to maintain attached flow on the entire main element, resulting in attached flow at the TE flap slot location. Otherwise, separation would take place upstream of the active slot, voiding its effectiveness, which relies on mixing enhancement. If the separated shear layer is remote from the active slot, communicated only by "dead" air, high-momentum fluid cannot be transported to the vicinity of the TE flap and its effectiveness would be low. Whereas Ref. 6 described the application of AFC to the LE flap shoulder, with the aim of maintaining attached flow on the main element up to $C_{L,\max}$, the majority of the current paper was devoted to AFC application on the TE flap upper surface. Effects attributed to surface curvature, increased BL thickness, and larger adverse pressure gradients significantly complicate AFC application at the TE flap region. Nonetheless, combined LE and TE flap AFC was attempted at low TE flap deflections where AFC benefits on the TE flap performance persisted to $C_{L,\max}$.

Figure 12 shows data combining the LE actuator with the flap actuator. The data presented are at $Re_c = 0.41 \times 10^6$ with $\delta_f = 5$ deg and $\delta_s = -25$ deg. The aft slot was used for introducing excitation on the TE flap because this slot is more effective than the other ones at $\delta_f = 5$ deg. The excitation frequencies were based on the resonant frequency of the actuators and in the case of LE excitation the AM frequency was chosen because it was the most effective at controlling separation. The C_μ values of the LE excitation were chosen based on the largest capable output using AM and the flap C_μ was the largest available for the flap actuator with the aft slot active. Excitation at the LE flap shoulder alone using $F^+ = 22$ is compared to excitation using $F^+ = 22$ with $F^+_{\mathrm{AM}} = 4$ (Fig. 12), showing slightly superior results due to the AM excitation. The flap actuator was operated at $F^+ = 5$ and excitation was introduced through the aft slot. Excitation C_μ values for the TE flap and LE flap actuators were 0.21 and 0.18%, respectively. Excitation at the LE flap shoulder ($x/c = 0.14\%$), using either the pure sine signal or the AM signal, increased $C_{L,\max}$ by 0.04 to 0.05 and delayed stall incidence by 2 deg (Fig. 12). Control applied from the aft slot of the flap actuator alone increased lift at stall by 0.03 but did not alter the stall angle. Note that increasing TE flap effectiveness or loading typically causes earlier TE flap stall. When the LE and TE excitations were combined, it resulted in similar gains in performance until $\alpha = 14$ deg, where $C_{L,\max}$ of the baseline was measured. However, the combination of pure sine, high-frequency excitation was more effective at larger α, increasing $C_{L,\max}$ to 2.1 and delaying stall to 16 deg. The larger effect of the high-frequency LE excitation combined with the TE excitation might be connected to the absence of large coherent structures generated by the LE low-frequency AM excitation, causing intermittently reversed flow at the the TE flap shoulder location.

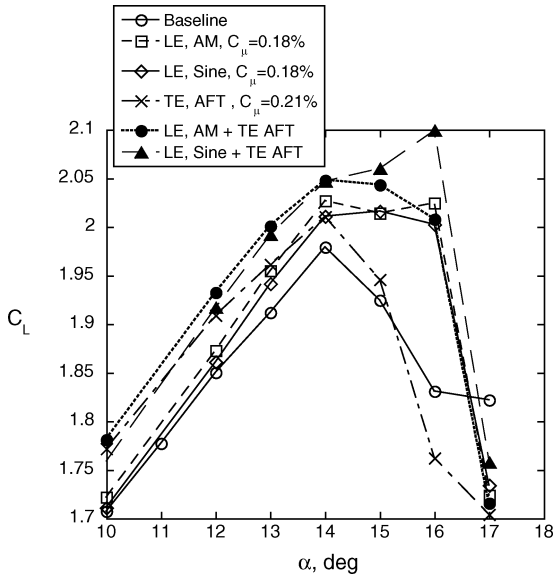

Fig. 12 Effect of LE and TE flap control on C_L ($Re_c = 0.41 \times 10^6$, $\delta_f = 5$ deg, $\delta_s = -25$ deg, $F^+_{\mathrm{LE}} = 22$, $F^+_{\mathrm{AM,LE}} = 4$, $F^+_{\mathrm{TE}} = 5$).

Conclusions

Although flow separation from the LE could be controlled using relatively low C_μ excitation, as reported in Ref. 6, controlling BL separation from the TE flap requires larger periodic momentum input. AM of the high-frequency excitation reduced the required C_μ by a factor of 3, a larger gain than what was found for the LE region excitation.

Curvature is believed to play an important role in the separation control process and the ratio between the resulting excitation wavelength and the radius of curvature of the surface might be a relevant parameter. The optimal TE flap defection for a particular excitation slot location on the TE flap changed significantly in regions of high surface curvature. Near the shoulder of the TE flap, where the surface is highly curved, a 3.2% chord change in the slot location caused a 30-deg change in the TE flap setting (δ_f) for maximum effectiveness. While in a region where the TE flap was not highly curved, a 9% chord change in the slot location caused only an 8 deg change in δ_f for maximum effectiveness.

Controlling separation at the LE and TE flap shoulders by combining multiple location excitations, when necessary, is the primary goal of this research. Preliminary data using combined LE and TE excitations indicate that increased airfoil performance can be obtained when control is applied simultaneously at both locations. LE control with AM excitation was more effective than high-frequency pure sine excitation when using the same C_μ. However, when the TE flap excitation was combined with the LE excitation, better performance was obtained when using high-frequency pure sine LE excitation. The physical understanding of the preceding finding requires further study.

Acknowledgments

The authors thank the following individuals for their support of the research program: Anna McGowan, William Sellers, Michael Walsh, Anthony Washburn, Luther Jenkins, John Lin, Norman Schaeffler, Richard White, George Hilton, Johnny Mau, Louis Hartzheim, Susan Palmer, and R. David Lewis.

References

[1]Greenblatt, D., and Wygnanski, I., "The Control of Flow Separation by Periodic Excitation," *Progress in Aerospace Science*, Vol. 36, No. 7, 2000, pp. 487–545.

[2]Nishri, B., and Wygnanski, I., "Effects of Periodic Excitation on Turbulent Flow Separation from a Flap," *AIAA Journal*, Vol. 36, No. 4, 1998, pp. 547–556.

[3]Seifert, A., Darabi, A., and Wygnanski, I., "On the Delay of Airfoil Stall by Periodic Excitation," *Journal of Aircraft*, Vol. 33, No. 4, 1996, pp. 691–699.

[4]Seifert, A., and Pack, L. G., "Oscillatory Control of Separation at High Reynolds Numbers," *AIAA Journal*, Vol. 37, No. 9, 1999, pp. 1062–1071.

[5]Seifert, A., and Pack, L. G., "Active Flow Separation Control on Wall-Mounted Hump at High Reynolds Numbers," *AIAA Journal*, Vol. 40, No. 7, 2002, pp. 1363–1372.

[6]Pack, L. G., Schaeffler, N. W., Yao, C., and Seifert, A., "Active Control of Separation from the Slat Shoulder of a Supercritical Airfoil," *Journal of Aircraft* (to be published).

[7]Seifert, A., Greenblatt, D., and Wygnanski, I., "Active Separation Control: Fundamental Principles, Current Status and Future Directions," *Aerospace Science and Technology*, Vol. 8, No. 1, 2004, pp. 569–589.

[8]McClean, J. D., Crouch, J. D., Stoner, R. C., Sakurai, S., and Feifel, G. E., Feifel, W. M., and Rush, H. M., "Study of the Application of Separation Control by Unsteady Excitation to Civil Transport Aircraft," NASA CR 1999-209338, 1999.

[9]Lin, J. C., and Dominik, C. J., "Parametric Investigation of a High-Lift Airfoil at High Reynolds Numbers," *Journal of Aircraft*, Vol. 34, No. 4, 1997, pp. 485–491.

[10]Abbott, I. H., and van Doenhoff, A., *Theory of Wing Sections*, Dover, New York, 1958, pp. 139–141.

[11]Naim, A., Greenblatt, D., Seifert, A., and Wygnanski, I., "Active Control of Cylinder Flow with and Without a Splitter Plate Using Piezoelectric Actuators," AIAA Paper 2002-3070, June 2002.

[12]Naim, A., "Active Control of Cylinder Flow with and Without a Splitter Plate," M.S. Thesis, Dept. of Fluid Mechanics and Heat Transfer, Tel-Aviv Univ., Ramat-Aviv, Israel, March 2003.

K. Fujii
Associate Editor